



Title	Non-coplanar spin structure in a metallic thin film of triangular lattice antiferromagnet CrSe
Author(s)	Tajima, Yusuke; Shiogai, Junichi; Ueda, Kohei et al.
Citation	APL Materials. 2024, 12, p. 041112
Version Type	VoR
URL	https://hdl.handle.net/11094/95775
rights	Copyright (2024) Author(s). This article is distributed under a Creative Commons Attribution (CC BY) License.
Note	





The University of Osaka Institutional Knowledge Archive : OUKA

<https://ir.library.osaka-u.ac.jp/>

The University of Osaka

RESEARCH ARTICLE | APRIL 10 2024

Non-coplanar spin structure in a metallic thin film of triangular lattice antiferromagnet CrSe


Yusuke Tajima; Junichi Shiogai ; Kohei Ueda ; Hirotake Suzuki; Kensuke Takaki; Takeshi Seki ; Kazutaka Kudo ; Jobu Matsuno 



APL Mater. 12, 041112 (2024)

<https://doi.org/10.1063/5.0201786>






APL Machine Learning

2023 Papers with Best Practices in Data Sharing and Comprehensive Background

Read Now



Non-coplanar spin structure in a metallic thin film of triangular lattice antiferromagnet CrSe

Cite as: APL Mater. 12, 041112 (2024); doi: 10.1063/5.0201786

Submitted: 31 January 2024 • Accepted: 25 March 2024 •

Published Online: 10 April 2024



Yusuke Tajima,¹ Junichi Shioyai,^{1,2,a)} Kohei Ueda,^{1,2} Hirotake Suzaki,¹ Kensuke Takaki,¹ Takeshi Seki,^{3,4} Kazutaka Kudo,^{1,2} and Jobu Matsuno^{1,2}

AFFILIATIONS

¹Department of Physics, Osaka University, Toyonaka, Osaka 560-0043, Japan

²Division of Spintronics Research Network, Institute for Open and Transdisciplinary Research Initiatives, Osaka University, Suita, Osaka 565-0871, Japan

³Institute for Materials Research, Tohoku University, Sendai 980-8577, Japan

⁴Center for Science and Innovation in Spintronics, Tohoku University, Sendai 980-8577, Japan

^{a)}Author to whom correspondence should be addressed: junichi.shioyai.sci@osaka-u.ac.jp

ABSTRACT

An antiferromagnetic metal with a two-dimensional triangular network offers a unique playground of intriguing magneto-transport properties and functionalities stemming from the interplay between conducting electrons and intricate magnetic phases. A NiAs-type CrSe is one of the candidates owing to alternate stackings of Cr and Se triangular atomic networks in its crystal structure. While the fabrication of CrSe thin films is indispensable to develop functional devices, studies on its thin-film properties have been limited to date due to the lack of metallic samples. Here, we report on the realization of metallic conductivities of CrSe thin films, which allows us to investigate their intrinsic magneto-transport properties. The metallic sample exhibits a co-occurrence of weak ferromagnetism with perpendicular magnetic anisotropy and antiferromagnetic behavior, indicating the presence of non-coplanar spin structures. In addition, control of the polarity and tilting angle of the non-coplanar spin structure is accomplished by a sign of cooling magnetic fields. The observed non-coplanar spin structure, which can be a source of emergent magnetic field acting on the conducting electrons, highlights the high potential of the triangular lattice antiferromagnet and provides a unique platform for functional thin-film devices composed of NiAs-type derivative Cr chalcogenides and pnictides.

© 2024 Author(s). All article content, except where otherwise noted, is licensed under a Creative Commons Attribution (CC BY) license (<https://creativecommons.org/licenses/by/4.0/>). <https://doi.org/10.1063/5.0201786>

I. INTRODUCTION

Triangular lattice antiferromagnets have long received attention owing to various magnetic states^{1,2} and related magneto-transport phenomena.^{3,4} A key feature of the triangular lattice antiferromagnets is the suppression of conventional long-range orders by geometrical frustration,^{5,6} which makes the system sensitive to magnetic anisotropy, thermal and quantum fluctuations, the external magnetic field, and other competing exchange interactions. When the frustrated spin system is subjected to these external stimuli, a rich variety of magnetic phases emerge, such as non-collinear⁷ and non-coplanar⁸ spin structures, magnetic skyrmion,^{9,10} a chiral spin liquid state,^{11,12} and disordered states known as spin glass states.^{13,14} Another intriguing feature, especially in

non-coplanar magnets, is the emergent magnetic field associated with the scalar spin chirality,³ which corresponds to a solid angle subtended by neighboring spins, so-called the real-space Berry phase.^{15,16} In some non-coplanar magnetic conductors, the connection of conducting electrons to the real-space emergent magnetic field is revealed as the topological Hall effect,^{10,17–20} non-reciprocal magneto-resistance,²¹ and electromagnetic induction.²² It has been suggested that the properties of those exotic spin textures can be enriched in nanostructures^{23–25} and heterointerfaces with conventional ferromagnets²⁶ or superconductors.²⁷ In this aspect, the exploration of magneto-transport properties in thin films composed of triangular lattice antiferromagnets is a central topic for further functionalization of their exotic magnetic properties and magnetoelectric effects.

The NiAs-type and its derivative compounds CrX ($X = S, Se, Te, \text{ and } Sb$) exhibit diverse magnetism depending on the choice of chalcogen and pnictogen elements.²⁸ For instance, CrTe shows ferromagnetism in bulk and thin-film forms, where ferromagnetic transition temperature and magnetic anisotropy can be tuned by the Cr and Te composition ratio.^{29–31} The CrSb has received recent attention as a new class of antiferromagnet, namely an altermagnet, in which the spin-split electronic band structure originates from not relativistic spin-orbit interaction but its crystal symmetry.^{32,33} Thanks to the large spin-splitting band, the altermagnet can be a candidate material as an efficient spin polarizer.³⁴ Among various types of magnetic materials, we focus on an antiferromagnetic CrSe, which has been long known as a triangular lattice antiferromagnet.³⁵ Figure 1(a) illustrates the crystal structure of the NiAs-type CrSe ($P6_3/mmc$) and the suggested Cr spin configuration. The Cr and Se two-dimensional triangular networks are alternately stacked along the c axis, while their spin structure has not been fully understood. The first neutron scattering experiment for CrSe reported that Cr spins in a basal plane are canted out toward the same direction,³⁵ forming the so-called umbrella-like spin structure as shown in Fig. 1(a). Later experiment performed for the NiAs-type derivative Cr_2Se_3 reported a more complex non-coplanar spin structure.³⁶ In the Cr–Se binary phase diagram, there are some equilibrium intermetallic phases: Cr_5Se_8 , Cr_2Se_3 , Cr_3Se_4 ,

and Cr_7Se_8 , all of which are in the NiAs-type derivative crystal structure with an ordered arrangement of Cr vacant sites,³⁷ and a high-temperature NiAs-type ($P6_3/mmc$) and its derivative ($P\bar{3}m1$) CrSe phases.³⁸ All binary phases at low and high temperatures have the same framework of crystal structure, where Cr atoms form edge-sharing and face-sharing $CrSe_6$ octahedra in the ab plane and along the c axis, respectively. The only differences between NiAs-type and its derivative Cr–Se compounds are the fraction and position of Cr deficient sites. The Néel temperature increases from 43, 82, and 280 K for Cr_2Se_3 , Cr_3Se_4 , and CrSe, respectively, in the order of the filling fraction of Cr sites.³⁹ As for the electrical transport properties, while metallic conduction has been reported in bulk single crystals,^{39–42} being consistent with semimetallic band structure in first-principles calculations,^{43,44} some experimental studies have reported semiconducting behavior in bulk^{45,46} and thin-film samples^{47–50} with a small bandgap (a few tens meV).^{46,47} This is probably because the Fermi level and/or bandgap are sensitive to a subtle off-stoichiometry or thickness in such a semimetal.^{43,44} In particular, thin-film samples reported so far have exhibited only semiconducting behavior,^{47–50} hindering explicit determination of the spin structure through the magneto-transport measurements. Nevertheless, some spin-related electrical transport experiments have been performed to date through the interfacial effects showing exchange bias,⁴⁸ the topological Hall effect,⁴⁹ and the magnetic

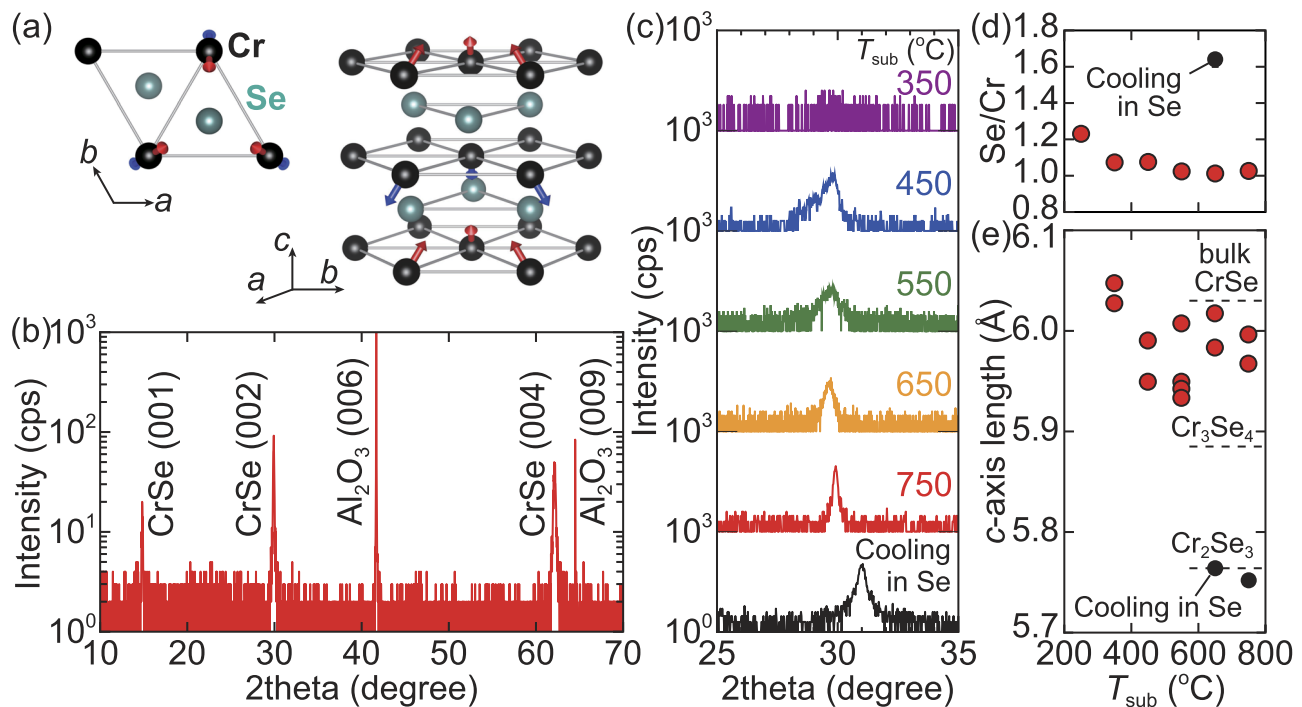


FIG. 1. Structural characterization of CrSe thin films. (a) Schematic crystal and spin structures of NiAs-type CrSe drawn by VESTA.⁶² Arrows illustrate Cr spins, which form a non-coplanar spin structure based on Ref. 35. (b) 2θ-ω scan of x-ray diffraction (XRD) pattern of Se-capped CrSe thin film grown at $T_{sub} = 750$ °C. (c) 2θ-ω XRD patterns around CrSe(002) for the CrSe thin films grown at $T_{sub} = 350$ (from top panel), 450, 550, 650, and 750 °C. As a reference, the XRD pattern of the Cr–Se thin film grown at $T_{sub} = 650$ °C and cooled under the Se ablation is shown in the bottom panel. The T_{sub} dependences of (d) Se/Cr chemical composition ratio and (e) c-axis length determined by the CrSe(002) XRD peak. Black circles correspond to the data points obtained by cooling in Se. The horizontal dashed lines in (e) indicate the bulk values of CrSe, Cr_3Se_4 , and Cr_2Se_3 , respectively.³⁷

proximity effect⁵⁰ between an insulating CrSe layer and conducting ferromagnetic or topological materials. Within the context of a non-coplanar spin structure having a scalar spin chirality, as mentioned earlier, preparation of the metallic CrSe thin films and exploration of magneto-transport properties should be tackled for an in-depth understanding of its spin structures.

In this article, we have found evolution toward metallic conduction in CrSe thin films by increasing growth temperature. Metallic conduction allows us to investigate the coupling of electric transport properties with spin structures via their magneto-transport measurements. From the magnetic-field and temperature dependences of longitudinal and Hall resistivities, the co-existence of a weak ferromagnetism with perpendicular magnetic anisotropy and an antiferromagnetic spin-flop transition accompanied by a memory effect was found in the metallic thin-film sample. We concluded that these features originate from a non-coplanar spin structure of CrSe.

II. EXPERIMENTAL METHODS

The CrSe thin films were grown on $\text{Al}_2\text{O}_3(0001)$ substrates by pulsed-laser deposition (PLD) at the substrate temperature $T_{\text{sub}} = 250, 350, 450, 550, 650, 750$, and 850°C . The CrSe and Se targets used in PLD were synthesized by pelletizing commercially available stoichiometric CrSe and Se powders (Kojundo Chemical Laboratory Co., Ltd.), respectively. For the electrical transport measurement, 50-nm-thick CrSe thin films were prepared, followed by the deposition of a 10-nm-thick amorphous Se cap layer at room temperature. For preparing the Se-rich sample as a reference, the Se target was ablated when the sample was cooled to room temperature after the CrSe thin film was grown at $T_{\text{sub}} = 650$ or 750°C . The chemical composition ratio (Se/Cr) of the thin-film samples was determined by energy dispersive x-ray spectroscopy (EDX) and inductively coupled plasma optical emission spectroscopy (ICP-OES). For the ICP analysis, the 100-nm-thick samples without the cap layer were prepared under identical growth conditions. The crystallinity was evaluated by x-ray diffraction and atomic force micrography (see supplementary material, Fig. S1), and thickness was determined by x-ray reflectivity (see supplementary material, Fig. S2).

Temperature and magnetic-field dependences of longitudinal and Hall resistivities were measured by standard five-terminal measurements in a ^4He cryostat equipped with a superconducting magnet (Oxford Instruments, plc). For subtracting the component of the ordinary Hall effect from $\rho_{yx}(H)$, a linear fit was applied for the high-field region in $\mu_0 H > 5$ T for the CrSe thin films grown at $T_{\text{sub}} = 350, 450, 550$, and 650°C and $\mu_0 H > 11$ T for $T_{\text{sub}} = 750^\circ\text{C}$. Magnetization measurements were performed by MPMS3 (Quantum Design, Inc.) with a superconducting quantum interference device.

III. RESULTS AND DISCUSSION

A. Thin film growth and structural characterization

Figure 1(b) shows a 2theta-omega scan of the x-ray diffraction (XRD) pattern of the Se-capped CrSe thin film for $T_{\text{sub}} = 750^\circ\text{C}$. Diffraction peaks from (00*n*) were clearly observed, while no other diffraction peaks from the film were detected, indicating single-phase and *c*-axis-orientated growth with negligible secondary

phase. Figure 1(c) shows the CrSe(002) diffraction peaks for T_{sub} from 350 to 750°C . Systematic dependence of the *c*-axis length on T_{sub} was not apparently observed. Note that any clear crystalline XRD patterns were not detected for $T_{\text{sub}} = 250$ and 850°C (see supplementary material, Fig. S3). The CrSe(002) diffraction peak for $T_{\text{sub}} = 650^\circ\text{C}$ with cooling in Se (denoted as “cooling in Se”) shifts toward a higher angle, indicating shrinkage of the *c*-axis length. Figures 1(d) and 1(e) summarize the T_{sub} dependence of the Se/Cr composition ratio and *c*-axis length, respectively. With increasing T_{sub} , the Se/Cr composition ratio monotonically decreases as expected from the high vapor pressure of Se and approaches the stoichiometric composition of CrSe. This trend is qualitatively consistent with the Cr–Se phase diagram,⁵¹ where the Se/Cr composition approaches unity toward high temperature. The *c*-axis lengths for all the CrSe thin films are comparable to the bulk value of NiAs-type CrSe [$P6_3/mmc$, $c = 6.030 \text{ \AA}$ (Ref. 37)]. In contrast, the *c*-axis length of CrSe thin film for $T_{\text{sub}} = 650$ and 750°C with cooling in Se was determined to be 5.764 and 5.752 \AA , respectively, and their Se/Cr ratio was about 1.6, which are comparable to the values of Cr_2Se_3 bulk single crystal [$I2/m$, $c = 5.764 \text{ \AA}$ (Ref. 37)]. Although further microscopic characterization and valence determination are necessary, it can be speculated that cooling in the Se-rich condition leads to the Cr_2Se_3 phase, while thin-film growth at $T_{\text{sub}} = 750^\circ\text{C}$ without excess Se causes stabilization of the high-temperature CrSe phase according to the analysis of the chemical composition and lattice constant.

B. Variation of electrical transport properties of CrSe thin films on growth temperature

Figure 2 shows the evolution of the electrical transport properties of CrSe thin films with an increase in T_{sub} . Figure 2(a) shows the T_{sub} dependences of Hall coefficient R_H (left axis) and longitudinal resistivity ρ_{xx} (right) measured at $T = 200 \text{ K}$. Here, the Hall coefficient, i.e., the inverse value of carrier density (n or $p = 1/eR_H$ with e being elementary charge), was extracted from

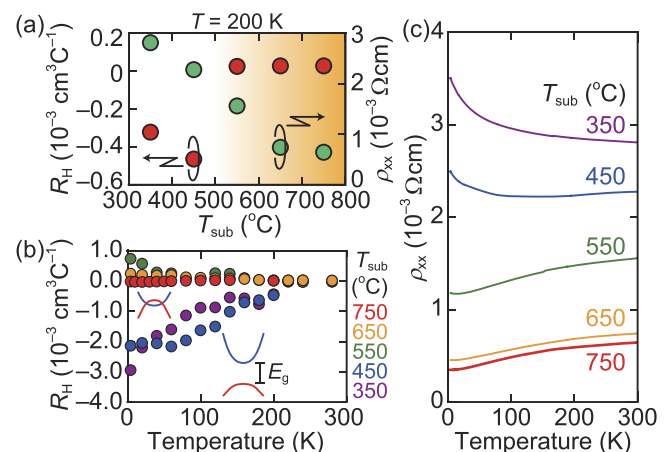


FIG. 2. Electrical transport characteristics. (a) Growth temperature T_{sub} dependence of high-field Hall coefficient R_H (red circles in the left axis) and resistivity ρ_{xx} (green circles in the right axis) measured at $T = 200 \text{ K}$. Temperature dependence of (b) R_H and (c) ρ_{xx} for $T_{\text{sub}} = 350$ (purple), 450 (blue), 550 (green), 650 (orange), and 750°C (red).

linear fits to the magnetic-field dependence of the Hall resistivity $\rho_{yx}(H)$ in the high-field range. In our definition, the negative and positive values of R_H correspond to electron and hole-dominated transport, respectively. For the low temperature growth at $T_{\text{sub}} = 350$ and 450°C , the R_H shows a negative value. With increasing T_{sub} above 550°C , the R_H changes its sign and does not show a significant variation with further increases in T_{sub} . Concomitantly, the value of ρ_{xx} at $T = 200$ K monotonically decreases with an increase in T_{sub} . The thermal variations of R_H for the CrSe films for various T_{sub} are shown in Fig. 2(b). The negative value of $R_H(T)$ for $T_{\text{sub}} = 350$ and 450°C shows a semiconducting dependence on T and reaches $R_H = -2.9$ and $-2.1 \times 10^{-3} \text{ cm}^3 \text{ C}^{-1}$ at $T = 4.2$ K, which corresponds to the electron density of 2.2 and $3.0 \times 10^{21} \text{ cm}^{-3}$, respectively. In contrast, the thermal variation of $R_H(T)$ for $T_{\text{sub}} = 550, 650$, and 750°C is not significant, which is typical behavior of semimetals composed of multiple bands such as CrTe (Ref. 31). The temperature dependence of longitudinal resistivities [$\rho_{xx}(T)$ curve] of the CrSe films for various T_{sub} is shown in Fig. 2(c). The CrSe thin films for $T_{\text{sub}} = 350$ and 450°C exhibit insulating or semiconducting behavior ($d\rho_{xx}/dT < 0$) in the whole temperature range, respectively, being consistent with the semiconducting $R_H(T)$ discussed in Fig. 2(b). Indeed, we can estimate the activation energy to be 16.8 meV from the $R_H(T)$ in the samples for $T_{\text{sub}} = 350^\circ\text{C}$ (see supplementary material, Fig. S4), which is comparable with a previously reported bandgap value of 34 meV in the thin-film sample.⁴⁷ Note that the insulating behavior of the $\rho_{xx}(T)$ curve of the CrSe-like thin film grown at low temperature is distinctly different from that for the Cr_2Se_3 -like thin film (cooling in Se): $\rho_{xx}(T)$ of the Cr_2Se_3 -like film more sharply increases at low temperature (see supplementary material, Fig. S5). For the higher T_{sub} samples, on the other hand, the $\rho_{xx}(T)$ exhibits metallic behaviors ($d\rho_{xx}/dT > 0$) down to the lowest temperature. Based on the temperature variation of R_H and ρ_{xx} , the series of CrSe thin-film samples can be distinguished into the low-temperature semiconducting phase for $T_{\text{sub}} = 350$ and 450°C and the high-temperature metallic phase for $T_{\text{sub}} = 550, 650$, and 750°C . Despite the significant structural difference not being detected from the present XRD analysis, we clearly observed an electronic phase transition by variation of the growth temperature. Further microscopic analysis may illustrate the link between NiAs-derivative crystal structures and electronic structures in high-temperature and low-temperature phases. Hereafter, we focus on the magneto-transport properties of the metallic CrSe thin film grown at 750°C .

C. Magneto-transport properties of metallic CrSe thin film

The impact of the spin structure on the electrical transport in CrSe was investigated by resistivity measurements of a metallic sample under a magnetic field. Figure 3(a) shows $\rho_{xx}(T)$ of the CrSe thin film for $T_{\text{sub}} = 750^\circ\text{C}$ under the out-of-plane magnetic field of $\mu_0 H = 0$ T [the same trace presented in Fig. 2(c)] and 14 T. Here, the magnetoresistance (MR) is defined as the difference of $\rho_{xx}(T)$ under $\mu_0 H$ given by $\Delta\rho_{xx}(T) = \rho_{xx}(T, \mu_0 H = 14 \text{ T}) - \rho_{xx}(T, \mu_0 H = 0 \text{ T})$. With decreasing T , the negative MR ($\Delta\rho_{xx} < 0$) appears at 180 K, which corresponds to the temperature where a kink was observed in $\rho_{xx}(T)$ at zero field (vertical dashed line). The coincidence of the kink feature, often assigned to the Néel temperature in metallic CrSe bulk

crystals,^{39,42} and the appearance of the negative MR at the same temperature suggests that the observed negative MR is a spin-related phenomenon. Figure 3(b) shows the temperature dependence of magnetization [$M(T)$ curve] measured at $\mu_0 H = 1$ T after 5 T field cooling (see supplementary material, Fig. S6). Despite the broad transition, the magnetization develops around $T \sim 180$ K, which further supports the relation between the kink and negative MR features in $\rho_{xx}(T)$ and the magnetic transition. In addition, the slope of the $M(T)$ curve becomes steeper below $T \sim 100$ K, implying that the perpendicular magnetic anisotropy with ferromagnetism develops, as will be discussed in Figs. 3(c) and 3(d). Nevertheless, the value of the measured magnetic moment is as small as $0.051 \mu_B/\text{Cr}$ at the lowest temperature. In the situation where Cr spins are aligned antiferromagnetically in the ab -plane, such a very small magnetic moment should originate from a projection of the canted Cr magnetic moments along the c axis. Considering the low-spin state of the $3d^4$ electron configuration of Cr^{2+} in CrSe, the residual moments of $0.051 \mu_B/\text{Cr}$ along the c axis out of the spin magnetic moment of $2 \mu_B/\text{Cr}$ yield a tilting angle of Cr spins from the basal plane of $\sin^{-1}(\frac{0.051}{2.0}) \sim 1.5^\circ$.

Figure 3(c) shows the out-of-plane magnetic-field dependence of the MR ratio at $T = 4.2, 20, 40, 100$, and 200 K. Here, we define the MR ratio as $\Delta\rho_{xx}/\rho_{xx}^0$, with $\Delta\rho_{xx} = \rho_{xx}(H) - \rho_{xx}^0$ and $\rho_{xx}^0 = \rho_{xx}(0)$. At $T = 200$ K, above the transition temperature of 180 K, the $\Delta\rho_{xx}/\rho_{xx}^0$ exhibited a negative and parabolic dependence. The negative MR becomes more significant at $T = 100$ K, and a butterfly-shaped hysteresis clearly emerges when decreasing T below 40 K, signaling the development of a ferromagnetic order. It is worth noting that hysteresis in $\Delta\rho_{xx}/\rho_{xx}^0$ was observed in a very wide range of magnetic fields up to 14 T at $T = 4.2$ K, which is extraordinarily larger than characteristic magnetic fields such as coercivity and saturation magnetic fields of the typical ferromagnetic compounds.^{30,31} The non-saturating negative MR can be ascribed to the suppression of spin scattering due to the reorientation of antiferromagnetically coupled spins.^{45,52} Figure 3(d) shows the magnetic-field dependence of the anomalous Hall resistivity $\rho_{yx}^A(H)$ obtained by subtracting the H -linear component from $\rho_{yx}(H)$ as a contribution from the ordinary Hall effect. The consistent hysteretic behavior of $\rho_{xx}(H)$ and $\rho_{yx}^A(H)$, accompanied by a small fraction of remanent $\rho_{yx}^A(0)$, was observed below $T = 100$ K, which indicates the development of spontaneous ferromagnetism along the c axis and is consistent with the steep increase of magnetization below that temperature, as shown in Fig. 3(b). The temperature dependence of the anomalous Hall effect is discussed in supplementary material, Fig. S7. The $\rho_{yx}^A(H)$ at $T = 4.2$ K exhibits the non-monotonic hump character around 5 T, which cannot be assigned to the anomalous Hall effect due to the magnetic-field dependence of the net out-of-plane magnetic moment. In the framework of the real-space Berry phase picture, the emergent magnetic field is developed by non-coplanar spin structures, which results in the non-monotonic hump structure, so-called the topological Hall effect.^{17,20} Indeed, the observation of the non-monotonic $\rho_{yx}^A(H)$ is consistent with the topological Hall effect, suggesting the presence of a non-coplanar spin structure in our CrSe thin film.

For interpretation of the intricate behaviors of $\rho_{xx}(H)$ and $\rho_{yx}^A(H)$, the angular dependence of MR was measured. Figure 3(e)

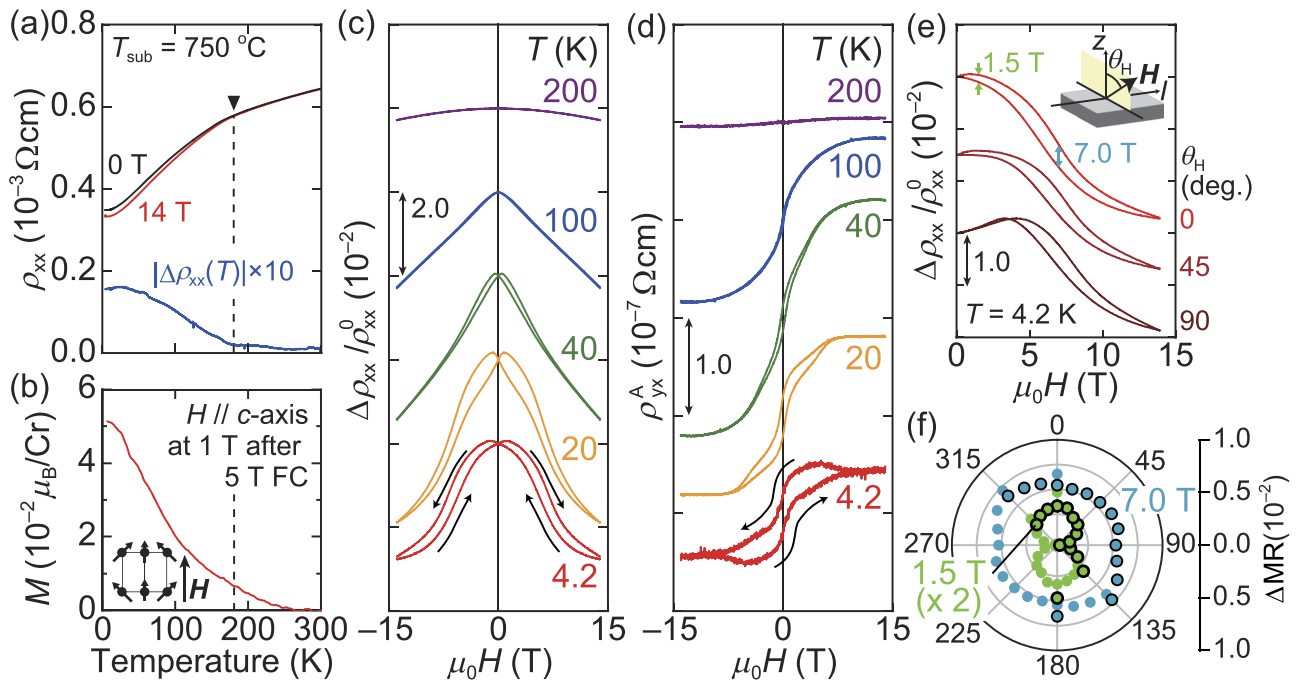


FIG. 3. Magneto-transport properties of the metallic CrSe thin film. (a) Temperature dependence of resistivity ρ_{xx} under zero field (black) and 14 T magnetic field (red). The absolute difference between the values of ρ_{xx} at 0 and 14 T is plotted in a blue solid line, where the vertical scale is multiplied by 10 for clarity. (b) Temperature dependence of magnetization at 1 T after 5 T field cooling (FC). (c) Magneto-resistance defined as $\Delta\rho_{xx}/\rho_{xx}^0$ and (d) magnetic-field dependence of anomalous Hall resistivity ρ_{yx}^A at $T = 4.2$ (red), 20 (orange), 40 (green), 100 (blue), and 200 K (purple). Here, $\Delta\rho_{xx}(H)$ and ρ_{xx}^0 represent $\rho_{xx}(H) - \rho_{xx}(0)$ and $\rho_{xx}(0)$. The $\Delta\rho_{xx}(H)/\rho_{xx}^0$ and $\rho_{yx}^A(H)$ curves are vertically offset for clarity. (e) $\Delta\rho_{xx}/\rho_{xx}^0(H)$ for different magnetic-field angles $\theta_H = 0^\circ, 45^\circ$, and 90° with respect to the normal to the plane and being fixed perpendicular to the electric current at 4.2 K. (f) Polar plot of ΔMR , which is defined as the difference in $\Delta\rho_{xx}/\rho_{xx}^0$ for upward and downward sweeps at 1.5 T (light green circles with black border) and 7.0 T (cyan circles with black border). The light green and cyan circles without a black border are obtained by replotting the data for θ_H on $\theta_H + 180^\circ$. Note that the radial scale of $\Delta\rho_{xx}/\rho_{xx}^0$ for 1.5 T is doubled for clarity.

shows the MR ratios $\Delta\rho_{xx}/\rho_{xx}^0$ for the angles $\theta = 0^\circ, 45^\circ$, and 90° . Here, θ_H is defined as the angle from the normal direction to the sample plane, and H is fixed perpendicular to the electric current. Interestingly, for the in-plane sweep ($\theta_H = 90^\circ$), the $\Delta\rho_{xx}/\rho_{xx}^0$ for upward and downward sweeps collapses in the low-field regime ($\mu_0 H < 3$ T) and exhibits a positive MR, while the hysteretic behavior remains in the high-field regime. The drastic change in the low-field MR with respect to θ_H is more visible in polar plots of ΔMR at $\mu_0 H = 1.5$ and 7.0 T, as shown in Fig. 3(f). Here, ΔMR is defined by the difference between the values of $\Delta\rho_{xx}/\rho_{xx}^0$ for the upward and downward sweeps [green and blue arrows in Fig. 3(e)]. The low-field ΔMR (at $\mu_0 H = 1.5$ T) exhibits strongly uniaxial anisotropy. For the high-field MR (at $\mu_0 H = 7.0$ T), in contrast, the ΔMR shows less anisotropic dependence. The distinct difference in low-field and high-field MR in θ_H dependence recalls the presence of two magnetic interactions with different magnetic anisotropy. By considering the remanent anomalous Hall resistivity in Fig. 3(d), the low-field MR comes from the weak but spontaneous ferromagnetism from the canted Cr spins toward the c -axis direction, which are ferromagnetically coupled between the basal planes. In contrast, we consider the nearly isotropic high-field component of MR, with its hysteresis closing at a very high magnetic field, to be the

character of triangular antiferromagnets. When antiferromagnets are magnetized by a sufficiently strong magnetic field, antiferromagnetically coupled spins undergo flops accompanied by a sudden rotation of the Néel vector, which renders distinct anomalies in magnetic and MR properties.^{53–55} Such a spin-flop transition usually occurs only when the field is applied along the well-defined spin axis in collinear antiferromagnets. In the case of triangular antiferromagnets with competing interplane interactions, however, it is suggested that a spin-flop transition may occur when the field is applied both parallel and perpendicular to the antiferromagnetic plane.^{56,57} The step-like and hysteretic behavior in negative MR implies a first-order nature of this magnetic transition. Another possibility is a spin-glass state, which emerges when the geometrical frustration is subjected to some amount of site disorders,⁵⁸ leading to a broad and unsaturated MR.⁵⁹ More detailed spin structure may be clarified by magnetization and magneto-transport measurement using high-field facilities.

In the presence of competing interplane weak ferromagnetism and intraplane geometrical frustration, the canting angle at a low temperature should depend on its history,^{60,61} in particular, the magnetic field applied when the system was frozen. Figure 4 shows the out-of-plane MR at 4.2 K starting from the “unmagnetized” state

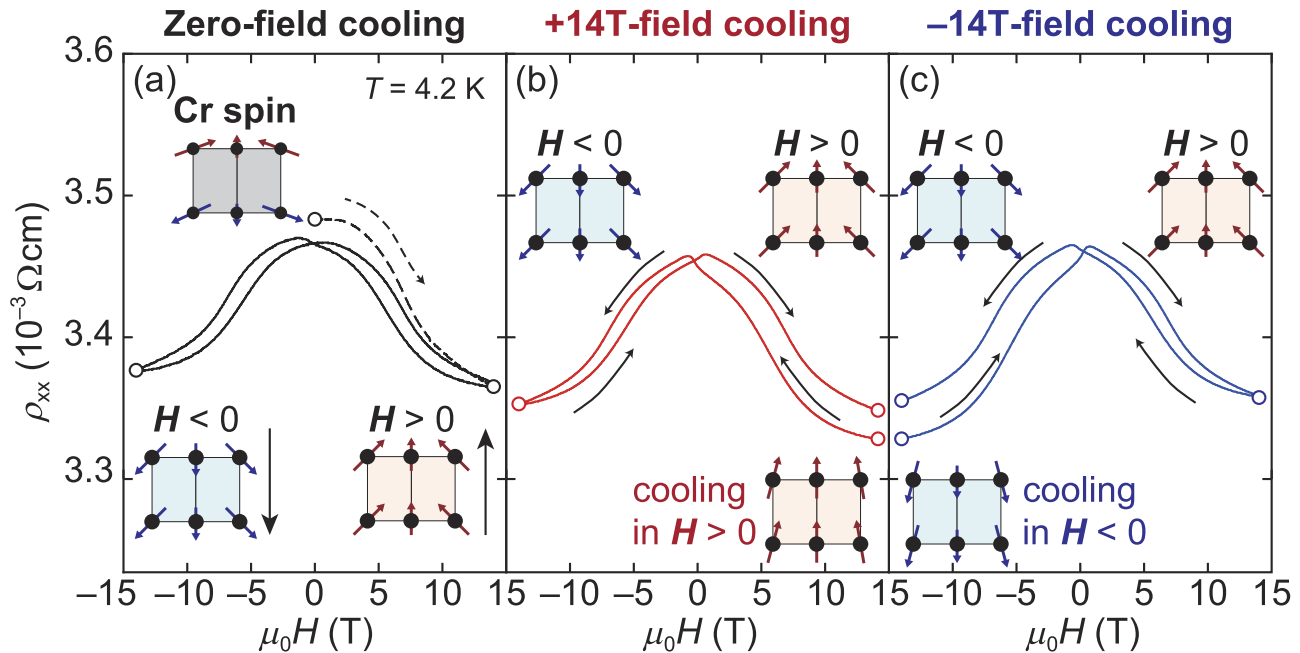


FIG. 4. Magnetic-field dependence of resistivity after (a) zero-field cooling, (b) field cooling at +14 T, and (c) field cooling at -14 T. The dashed line in (a) represents the initial curve obtained after the zero-field cooling. The inset shows schematics of the proposed Cr spin structure at each magnetic field represented by the open circles (not to scale).

obtained by zero-field cooling (ZFC) [Fig. 4(a)] and “magnetized” states by +14 and -14 T field cooling (FC) [Figs. 4(b) and 4(c)], respectively. The $\rho_{xx}(H)$ obtained from ZFC shows the negative MR from the initial state up to 14 T and exhibits an almost symmetric shape with respect to zero magnetic field. In this situation, the magnetic field drives the spin-flop transition from the compensated antiferromagnetic state after ZFC into a weak ferromagnetic phase, as schematically shown in the insets. Please note that a small asymmetric composition may come from the superposition of $\rho_{yx}(H)$. In contrast, the $\rho_{xx}(H)$ obtained from the +14 T-FC consists of an asymmetric component in addition to the negative MR, as shown in Fig. 4(b). The initial value of ρ_{xx} at +14 T shows a lower resistivity than that for the ZFC. After a cycling magnetic field between +14 T and -14 T, ρ_{xx} at +14 T returns to a comparable value to that obtained in ZFC. While the negative MR is independent of the polarity of the cooling field, we found that the sign of the asymmetric component is inverted by the polarity change of the field, as shown in Fig. 4(c). This memory effect in MR polarities under the perpendicular magnetic field implies that the magnetic field in FC more effectively acts on the system than in ZFC to force the magnetic moment along the field. The observed non-saturating negative magnetoresistance, accompanied by the memory effect, implies antiferromagnetic features as reported in various non-coplanar and non-collinear antiferromagnetic conductors.^{45,59,60}

By considering the co-occurrence of weak ferromagnetism with uniaxial anisotropy perpendicular to the basal planes and the antiferromagnetic features, we conclude that our metallic CrSe

thin film possesses the non-coplanar spin structure as one of the ground states in antiferromagnetically coupled Cr triangular networks. It turns out that the polarity and canting angle of the Cr spins, which are sources of the real-space emergent magnetic field, can be tuned by cooling under the magnetic field.

IV. SUMMARY AND OUTLOOK

In summary, we have obtained a semiconductor-to-metal transition in CrSe thin films by increasing the growth temperature. The metallic CrSe thin film exhibits hysteretic negative magnetoresistance, remanent anomalous Hall resistivity, and the small Cr magnetic moment when the perpendicular magnetic field is applied, revealing the presence of the weak ferromagnetic order with perpendicular magnetic anisotropy. In addition, unsaturated and isotropic hysteretic magnetoresistance showing the memory effect is reminiscent of the competition between intraplane geometrical frustration and interplane coupling. The co-existence of weak ferromagnetism along perpendicular to the basal plane and geometrical frustration within the plane indeed suggests the presence of the non-coplanar spin structure in the two-dimensional triangular lattice. Considering the rich variety of magnetic states exhibited in the NiAs-type and its derivative Cr chalcogenides and pnictides, our observation of the non-coplanar spin structure in the CrSe thin film offers a unique platform to tailor intricate magnetic interaction and spintronic functionalities in the NiAs-based thin-film and heterostructure devices.

SUPPLEMENTARY MATERIAL

See the supplementary material for additional structural characterization, bandgap estimation for the semiconducting CrSe thin films, electrical transport properties of the Cr₂Se₃-like thin film, analysis of magnetization measurements, and temperature dependence of anomalous Hall conductivity.

ACKNOWLEDGMENTS

The authors acknowledge Masaki Nakano for the fruitful discussion. This work was partly performed under the GIMRT Program of the Institute for Materials Research, Tohoku University (Proposal No. 202212-CRKEQ-0007). The ICP-OES analysis was carried out by Shigeru Tamiya at the Osaka University Core Facility Center as a part of the MEXT Project for promoting public utilization of advanced research infrastructure (a program for supporting the construction of core facilities), Grant No. JPMXS0441200023. This work was supported by JSPS KAKENHI Grant Nos. JP21K18889, JP23H01686, JP19H05823, and JP22H01182.

AUTHOR DECLARATIONS

Conflict of Interest

The authors have no conflicts to disclose.

Author Contributions

Yusuke Tajima: Data curation (lead); Formal analysis (equal); Visualization (equal); Writing – original draft (equal). **Junichi Shiogai:** Conceptualization (lead); Formal analysis (equal); Funding acquisition (equal); Supervision (equal); Visualization (equal); Writing – original draft (equal). **Kohei Ueda:** Writing – review & editing (equal). **Hirotake Suzuki:** Methodology (equal). **Kensuke Takaki:** Methodology (equal). **Takeshi Seki:** Methodology (equal); Writing – review & editing (equal). **Kazutaka Kudo:** Funding acquisition (equal); Methodology (equal); Writing – review & editing (equal). **Jobu Matsuno:** Methodology (equal); Supervision (equal); Writing – review & editing (equal).

DATA AVAILABILITY

The data that support the findings of this study are available from the corresponding author upon reasonable request.

REFERENCES

- ¹A. V. Chubukov and D. I. Golosov, “Quantum theory of an antiferromagnet on a triangular lattice in a magnetic field,” *J. Phys.: Condens. Matter* **3**, 69 (1991).
- ²D. Yamamoto, T. Sakurai, R. Okuto, S. Okubo, H. Ohta, H. Tanaka, and Y. Uwatoko, “Continuous control of classical-quantum crossover by external high pressure in the coupled chain compound CsCuCl₃,” *Nat. Commun.* **12**, 4263 (2021).
- ³N. Nagaosa and Y. Tokura, “Emergent electromagnetism in solids,” *Phys. Scr.* **T146**, 014020 (2012).
- ⁴S. Nakatsuji, N. Kiyohara, and T. Higo, “Large anomalous Hall effect in a non-collinear antiferromagnet at room temperature,” *Nature* **527**, 212 (2015).

- ⁵A. P. Ramirez, “Strongly geometrically frustrated magnets,” *Annu. Rev. Mater. Res.* **24**, 453 (1994).
- ⁶C. Nisoli, R. Moessner, and P. Schiffer, “Colloquium: Artificial spin ice: Designing and imaging magnetic frustration,” *Rev. Mod. Phys.* **85**, 1473 (2013).
- ⁷K. Kubo and T. Z. Momoi, “Ground state of a spin system with two- and four-spin exchange interactions on the triangular lattice,” *Z. Phys. B: Condens. Matter* **103**, 485 (1997).
- ⁸R. Shindou and N. Nagaosa, “Orbital ferromagnetism and anomalous Hall effect in antiferromagnets on the distorted fcc lattice,” *Phys. Rev. Lett.* **87**, 116801 (2001).
- ⁹Y. Tokura and N. Kanazawa, “Magnetic skyrmion materials,” *Chem. Rev.* **121**, 2857 (2021).
- ¹⁰T. Kurumaji, T. Nakajima, M. Hirschberger, A. Kikkawa, Y. Yamasaki, H. Sagayama, H. Nakao, Y. Taguchi, T. Arima, and Y. Tokura, “Skyrmion lattice with a giant topological Hall effect in a frustrated triangular-lattice magnet,” *Science* **365**, 914 (2019).
- ¹¹V. Kalmeyer and R. B. Laughlin, “Equivalence of the resonating-valence-bond and fractional quantum Hall states,” *Phys. Rev. Lett.* **59**, 2095 (1987).
- ¹²Y. Zhou, K. Kanoda, and T. K. Ng, “Quantum spin liquid states,” *Rev. Mod. Phys.* **89**, 025003 (2017).
- ¹³K. Binder and A. P. Young, “Spin glasses: Experimental facts, theoretical concepts, and open questions,” *Rev. Mod. Phys.* **58**, 801 (1986).
- ¹⁴U. Kamber, A. Bergman, A. Eich, D. Iuşan, M. Steinbrecher, N. Hauptmann, L. Nordström, M. I. Katsnelson, D. Wegner, O. Eriksson, and A. A. Khajetoorians, “Self-induced spin glass state in elemental and crystalline neodymium,” *Science* **368**, 6494 (2020).
- ¹⁵J. Ye, Y. B. Kim, A. J. Millis, B. I. Shraiman, P. Majumdar, and Z. Tešanović, “Berry phase theory of the anomalous Hall effect: Application to colossal magnetoresistance manganites,” *Phys. Rev. Lett.* **83**, 3737 (1999).
- ¹⁶K. Ohgushi, S. Murakami, and N. Nagaosa, “Spin anisotropy and quantum Hall effect in the *kagomé* lattice: Chiral spin state based on a ferromagnet,” *Phys. Rev. B* **62**, R6065 (2000).
- ¹⁷Y. Taguchi, Y. Oohara, H. Yoshizawa, N. Nagaosa, and Y. Tokura, “Spin chirality, Berry phase, and anomalous Hall effect in a frustrated ferromagnet,” *Science* **291**, 2573 (2001).
- ¹⁸J. Matsuno, N. Ogawa, K. Yasuda, F. Kagawa, W. Koshibae, N. Nagaosa, Y. Tokura, and M. Kawasaki, “Interface-driven topological Hall effect in SrRuO₃-SrIrO₃ bilayer,” *Sci. Adv.* **2**, e1600304 (2016).
- ¹⁹Y. Ohuchi, J. Matsuno, N. Ogawa, Y. Kozuka, M. Uchida, Y. Tokura, and M. Kawasaki, “Electric-field control of anomalous and topological Hall effects in oxide bilayer thin films,” *Nat. Commun.* **9**, 213 (2018).
- ²⁰A. Neubauer, C. Pfleiderer, B. Binz, A. Rosch, R. Ritz, P. G. Niklowitz, and P. Böni, “Topological Hall effect in the A phase of MnSi,” *Phys. Rev. Lett.* **102**, 186602 (2009).
- ²¹T. Yokouchi, N. Kanazawa, A. Kikkawa, D. Morikawa, K. Shibata, T. Arima, Y. Taguchi, F. Kagawa, and Y. Tokura, “Electrical magnetochiral effect induced by chiral spin fluctuations,” *Nat. Commun.* **8**, 866 (2017).
- ²²T. Schulz, R. Ritz, A. Bauer, M. Halder, M. Wagner, C. Franz, C. Pfleiderer, K. Everschor, M. Garst, and A. Rosch, “Emergent electrodynamics of skyrmions in a chiral magnet,” *Nat. Phys.* **8**, 301 (2012).
- ²³A. O. Leonov and M. Mostovoy, “Edge states and skyrmion dynamics in nanostripes of frustrated magnets,” *Nat. Commun.* **8**, 14394 (2017).
- ²⁴P. Bruno, V. K. Dugaev, and M. Taillefumier, “Topological Hall effect and Berry phase in magnetic nanostructures,” *Phys. Rev. Lett.* **93**, 096806 (2004).
- ²⁵N. Kanazawa, M. Kubota, A. Tsukazaki, Y. Kozuka, K. S. Takahashi, M. Kawasaki, M. Ichikawa, F. Kagawa, and Y. Tokura, “Discretized topological Hall effect emerging from skyrmions in constricted geometry,” *Phys. Rev. B* **91**, 041122 (2015).
- ²⁶F. J. Morvan, H. B. Luo, H. X. Yang, X. Zhang, Y. Zhou, G. P. Zhao, W. X. Xia, and J. P. Liu, “An achiral ferromagnetic/chiral antiferromagnetic bilayer system leading to controllable size and density of skyrmions,” *Sci. Rep.* **9**, 2970 (2019).
- ²⁷X. G. Wen, F. Wilczek, and A. Zee, “Chiral spin states and superconductivity,” *Phys. Rev. B* **39**, 11413 (1989).
- ²⁸K. Adachi, “Magnetic anisotropy energy in nickel arsenide type crystals,” *J. Phys. Soc. Jpn.* **16**, 2187 (1961).

- ²⁹H. Ipser, K. L. Komarek, and K. O. Klepp, "Transition metal-chalcogen systems viii: The Cr-Te phase diagram," *J. Less-Common Met.* **92**, 265 (1983).
- ³⁰Y. Fujisawa, M. Pardo-Almanza, J. Garland, K. Yamagami, X. Zhu, X. Chen, K. Araki, T. Takeda, M. Kobayashi, Y. Takeda, C. H. Hsu, F. C. Chuang, R. Laskowski, K. H. Khoo, A. Soumyanarayanan, and Y. Okada, "Tailoring magnetism in self-intercalated $\text{Cr}_{1+\delta}\text{Te}_2$ epitaxial films," *Phys. Rev. Mater.* **4**, 114001 (2020).
- ³¹Y. Wang, S. Kajihara, H. Matsuoka, B. K. Saika, K. Yamagami, Y. Takeda, H. Wadati, K. Ishizaka, Y. Iwasa, and M. Nakano, "Layer-number-independent two-dimensional ferromagnetism in Cr_3Te_4 ," *Nano Lett.* **22**, 9964 (2022).
- ³²L. Šmejkal, J. Sinova, and T. Jungwirth, "Emerging research landscape of altermagnetism," *Phys. Rev. X* **12**, 040501 (2022).
- ³³S. Reimers, L. Odenbreit, L. Šmejkal, V. N. Strocov, P. Constantinou, A. B. Hellenes, R. J. Ubierto, W. H. Campos, V. K. Bharadwaj, A. Chakraborty, T. Denneulin, W. Shi, R. E. Dunin-Borkowski, S. Das, M. Kläui, J. Sinova, and M. Jourdan, "Direct observation of altermagnetic band splitting in CrSb thin films," *Nat. Commun.* **15**, 2116 (2024).
- ³⁴R. González-Hernández, L. Šmejkal, K. Výborný, Y. Yahagi, J. Sinova, T. Jungwirth, and J. Železný, "Efficient electrical spin splitter based on nonrelativistic collinear antiferromagnetism," *Phys. Rev. Lett.* **126**, 127701 (2021).
- ³⁵L. M. Corliss, N. Elliott, J. M. Hastings, and R. L. Sass, "Magnetic structure of chromium selenide," *Phys. Rev.* **122**, 1402 (1961).
- ³⁶Y. Adachi, M. Ohashi, T. Kaneko, M. Yuzuri, Y. Yamaguchi, S. Funahashi, and Y. Morii, "Magnetic structure of rhombohedral Cr_2Se_3 ," *J. Phys. Soc. Jpn.* **63**, 1548 (1994).
- ³⁷F. H. Wehmeier, E. T. Keve, and S. C. Abrahams, "Preparation, structure, and properties of some chromium selenides. Crystal growth with selenium vapor as a novel transport agent," *Inorg. Chem.* **9**, 2125 (1970).
- ³⁸I. Tsubokawa, "The magnetic properties of single crystals of chromium selenide," *J. Phys. Soc. Jpn.* **15**, 2243 (1960).
- ³⁹S. Ohta, Y. Narui, and M. Ohwatari, "Electrical properties of $\text{Cr}_{1-\delta}\text{Se}$ ($0.07 \leq \delta \leq 0.33$)," *J. Phys. Soc. Jpn.* **65**, 3084 (1996).
- ⁴⁰Y. Adachi, K. Izaki, K. Koike, H. Morita, T. Kaneko, H. Kimura, and A. Inoue, "Electrical resistivity and magnetic property for Cr_2Se_3 and its Te-substitution system," *J. Magn. Magn. Mater.* **310**, 1849 (2007).
- ⁴¹Y. B. Li, Y. Q. Zhang, W. F. Li, D. Li, J. Li, and Z. D. Zhang, "Spin-glass-like behavior and electrical transport properties of $\text{Cr}_7(\text{Se}_{1-x}\text{Te}_x)_8$," *Phys. Rev. B* **73**, 212403 (2006).
- ⁴²J. Wu, C. L. Zhang, J. M. Yan, L. Chen, L. Guo, T. W. Chen, G. Y. Gao, L. Fei, W. Zhao, Y. Chai, and R. K. Zheng, "Magnetotransport and magnetic properties of the layered noncollinear antiferromagnetic Cr_2Se_3 single crystals," *J. Phys.: Condens. Matter* **32**, 475801 (2020).
- ⁴³J. Dijkstra, C. F. van Bruggen, C. Haas, and R. A. de Groot, "Band-structure calculations, and magnetic and transport properties of ferromagnetic chromium tellurides (CrTe , Cr_3Te_4 , Cr_2Te_3)," *J. Phys.: Condens. Matter* **1**, 9163 (1989).
- ⁴⁴Y. Gebredingle, M. Joe, and C. Lee, "First-principles calculations of the spin-dependent electronic structure and strain tunability in 2D non-van der Waals chromium chalcogenides Cr_2X_3 ($\text{X} = \text{S}, \text{Se}, \text{Te}$): Implications for spintronics applications," *ACS Appl. Nano Mater.* **5**, 10383 (2022).
- ⁴⁵S. J. Zhang, J. M. Yan, F. Tang, J. Wu, W. Q. Dong, D. W. Zhang, F. S. Luo, L. Chen, Y. Fang, T. Zhang, Y. Chai, W. Zhao, X. Wang, and R. K. Zheng, "Colossal magnetoresistance in Ti lightly doped Cr_2Se_3 single crystals with a layered structure," *ACS Appl. Mater. Interfaces* **13**, 58949 (2021).
- ⁴⁶J. Yan, X. Luo, F. C. Chen, Q. L. Pei, G. T. Lin, Y. Y. Han, L. Hu, P. Tong, W. H. Song, X. B. Zhu, and Y. P. Sun, "Anomalous Hall effect in two-dimensional non-collinear antiferromagnetic semiconductor $\text{Cr}_{0.68}\text{Se}$," *Appl. Phys. Lett.* **111**, 022401 (2017).
- ⁴⁷A. Roy, R. Dey, T. Pramanik, A. Rai, R. Schalap, S. Majumder, S. Guchhait, and S. K. Banerjee, "Structural and magnetic properties of molecular beam epitaxy grown chromium selenide thin films," *Phys. Rev. Mater.* **4**, 025001 (2020).
- ⁴⁸C. Wang, B. Zhang, B. You, S. K. Lok, S. K. Chan, X. X. Zhang, G. K. L. Wong, and I. K. Sou, "Molecular-beam-epitaxy-grown CrSe/Fe bilayer on $\text{GaAs}(100)$ substrate," *J. Appl. Phys.* **102**, 083901 (2007).
- ⁴⁹J. H. Jeon, H. R. Na, H. Kim, S. Lee, S. Song, J. Kim, S. Park, J. Kim, H. Noh, G. Kim, S. K. Jerng, and S. H. Chun, "Emergent topological Hall effect from exchange coupling in ferromagnetic Cr_2Te_3 /noncoplanar antiferromagnetic Cr_2Se_3 bilayers," *ACS Nano* **16**, 8974 (2022).
- ⁵⁰C. Y. Yang, L. Pan, A. J. Grutter, H. Wang, X. Che, Q. L. He, Y. Wu, D. A. Gilbert, P. Shafer, E. Arenholz, H. Wu, G. Yin, P. Deng, J. A. Borchers, W. Ratcliff II, and K. L. Wang, "Termination switching of antiferromagnetic proximity effect in topological insulator," *Sci. Adv.* **6**, eaaz8463 (2020).
- ⁵¹H. Okamoto, *Data Handbook: Phase Diagrams for Binary Alloys*, 2nd ed. (ASM International, Materials Park, OH, USA, 1990).
- ⁵²J. Y. Chan, S. M. Kauzlarich, P. Klavins, R. N. Shelton, and D. J. Webb, "Colossal negative magnetoresistance in an antiferromagnet," *Phys. Rev. B* **57**, R8103(R) (1998).
- ⁵³Y. Deng, Y. Yu, M. Z. Shi, Z. Guo, Z. Xu, J. Wang, X. H. Chen, and Y. Zhang, "Quantum anomalous Hall effect in intrinsic magnetic topological insulator MnBi_2Te_4 ," *Science* **367**, 895 (2020).
- ⁵⁴J. Wang, J. Deng, X. Liang, G. Gao, T. Ying, S. Tian, H. Lei, Y. Song, X. Chen, J. Guo, and X. Chen, "Spin-flip-driven giant magnetotransport in A-type antiferromagnet NaCrTe_2 ," *Phys. Rev. Mater.* **5**, L091401 (2021).
- ⁵⁵D. G. Oh, J. H. Kim, M. K. Kim, K. W. Jeong, H. J. Shin, J. M. Hong, J. S. Kim, K. Moon, N. Lee, and Y. J. Choi, "Spin-flip-driven anomalous Hall effect and anisotropic magnetoresistance in a layered Ising antiferromagnet," *Sci. Rep.* **13**, 3391 (2023).
- ⁵⁶T. Nikuni and H. Shiba, "Quantum fluctuations and magnetic structures of CsCuCl_3 in high magnetic field," *J. Phys. Soc. Jpn.* **62**, 3268 (1993).
- ⁵⁷Z. Jin, Z. C. Xia, M. Wei, J. H. Yang, B. Chen, S. Huang, C. Shang, H. Wu, X. X. Zhang, J. W. Huang, and Z. W. Ouyang, "3D spin-flop transition in enhanced 2D layered structure single crystalline TiCo_2Se_2 ," *J. Phys.: Condens. Matter* **28**, 396002 (2016).
- ⁵⁸P. A. Beck, "Properties of mictomagnets (spinglasses)," *Prog. Mater. Sci.* **23**, 1 (1980).
- ⁵⁹C. L. Canedy, K. B. Ibsen, G. Xiao, J. Z. Sun, A. Gupta, and W. J. Gallagher, "Magnetotransport and hysteretic behavior in epitaxial $\text{La}_{0.67}\text{Ca}_{0.33}\text{MnO}_{3-\delta}$ films," *J. Appl. Phys.* **79**, 4546 (1996).
- ⁶⁰T. C. Fujita, Y. Kozuka, M. Uchida, A. Tsukazaki, T. Arima, and M. Kawasaki, "Odd-parity magnetoresistance in pyrochlore iridate thin films with broken time-reversal symmetry," *Sci. Rep.* **5**, 9711 (2015).
- ⁶¹J. Nogués and I. K. Schuller, "Exchange bias," *J. Magn. Magn. Mater.* **192**, 203 (1999).
- ⁶²K. Momma and F. Izumi, "VESTA 3 for three-dimensional visualization of crystal, volumetric and morphology data," *J. Appl. Crystallogr.* **44**, 1272 (2011).